Proceedings of the 7th World Congress on Momentum, Heat and Mass Transfer (MHMT'22)
~~Lisbon, Portugal~~ Virtual Conference – April 07 – 09, 2022
Paper No. ICMFHT 148
DOI: 10.11159/icmfht22.148

Modeling the Carbon Black Production in Enclosed FSP Reactor

Fabio Henrique Bastiani[1], Pedro Bianchi Neto[1], Lizoel Buss[2,3], Udo Fritsching[2,3], Dirceu Noriler[1]
[1] Department of Process Engineering – DEPro, University of Campinas, Brazil
[2] Leibniz Institute for Materials Engineering - IWT, Bremen, Germany
[3] Department of Particles and Process Engineering, University of Bremen, Germany
*Corresponding author email: dnoriler@unicamp.br

Abstract **–** Carbon black is a high-interest industrial material due to its favorable characteristics and applications as nanoparticles. This substance is generated by combustion processes in diffusive or turbulent flames. Over the years, distinct models were developed and presented to model soot and carbon black formation kinetics in combustion chambers and reactors. One method to manufacture nanoparticles is the Flame Spray Pyrolysis process, with the advantage of offering a more controlled environment to tailor particle's properties. In this work, simulations of the FSP process are carried out considering the formation of carbon black nanoparticles. CFD simulations were performed approaching the continuous phase by an Eulerian framework and the dispersed phase (spray droplets) by a Lagrangian framework. A three-equation model is applied to predict the carbon black formation kinetics, and particle radiation is also considered. The injected fuel at the nozzle is composed of pure p-xylene. A 2D axisymmetric approach is considered to represent the enclosed FSP cylindrical reactor, and two different domains were investigated: with and without the surroundings of the reactor. Adiabatic and non-adiabatic wall cases are simulated to study the temperature and carbon black formation profiles. The influence of particle radiation is also analyzed. Results show that the insulated reactor (adiabatic wall) has a higher temperature profile along the reactor, affecting nucleation and oxidation rates of carbon black.

Keywords**:** Carbon Black, Flame Spray Pyrolysis, CFD, Fluent.

1. Introduction

The formation of soot and carbon black has been studied by several authors over the years and its formation mechanism still is an enigmatic subject. Many studies tried to understand and model the formation of soot, mainly for diesel engines [1]–[5], laminar/diffusion flames [6]–[8], and turbulent flames [9], [10]. Soot is a subproduct of combustion processes that arise from fuel-burning at high temperatures, being generated by incomplete combustion and aggregation of hydrocarbons.

The formation mechanism of soot is directly related to the formation of polycyclic aromatic hydrocarbons (PAHs) by many authors. As described by Frenklach and Wang [11], PAHs are a combination of several aromatic rings, generating aggregates with high molecular weight. The authors describe this reaction mechanism by two processes, the addition reaction of two aromatic rings and its growth by the addition of vinyl (C_2H_3) and acetylene (C_2H_2), which is named as HACA mechanism (hydrogen-abstraction-C_2H_2-addition) [8], [11], [12]. After the polycyclic aromatics are formed there are a few steps to generate soot particles, described in the literature as nucleation, superficial growth, and agglomeration [13]–[15]. By understanding these formation steps, it would be possible to mathematically model how soot is produced in combustion processes.

There is industrial interest in the production of carbon nanoparticles, but these particles are commonly divided into two categories: soot and carbon black. The former is a subproduct of combustion reactors, having a composition of 60% of pure carbon and, the latter is a purer form of soot, with compositions reaching 97% of elemental carbon [16]. Carbon black's production is of particular interest, due to its diverse applications. This material is mainly used as a rubber reinforcement on tires, although they are also mixed with modern battery slurry to increase life and battery performance [17]–[19].

In this study, we propose to simulate the manufacture of carbon black using the Flame Spray Pyrolysis (FSP) process, which is in fact, similar to the most common method of carbon black's producing, named furnace black [20]. The main advantage of using the FSP process is that its controlled environment allows one to control specific characteristics of the generated particles [21]. Features like electrical conductivity, superficial area, and particle size are directly related to its

manufacturing procedure. By controlling the FSP process parameters such as temperature, the air of co-flow, and fuel rate, it is possible to generate auspicious characteristics in the final product [22]–[26].

Flame spray pyrolysis is a well-known method for nanoparticle production and can manufacture particles of several elements from the periodic table. The process has important technological features such as the direct use of liquid feeds, proven scalability, and high-temperature flames and temperature gradients along the reactor [21]. The synthesized material's properties are determined and controlled by operating conditions and nozzle configuration, which brings different possibilities to nanoparticle production. By coupling computational fluid dynamics (CFD) with populational balance modeling (PBM) to describe particle dynamics, it is possible to simulate different conditions and predict relevant aspects of the process and the particles produced [25]. In this work, we carry out simulations with ANSYS Fluent 19.2, aiming to simulate carbon black production in an FSP reactor using different approaches and reactor configurations.

2. Simulation Setup

The reactor system is approximated by a 2D axisymmetric domain, where the continuous gas phase is represented by an Eulerian framework, and the dispersed evaporating droplets by a Lagrangian framework, with two-way coupling between phases. Steady-state and compressible flow conditions are considered, and turbulence is calculated with a k-ω SST model, as described in the works of Bianchi Neto, et al. [26].

A numerical mesh, with approximately 200.000 hexahedral elements, is used in the discretization of the domain that consists of a cylindrical reactor (surrounded by a glass tube) with 500 mm of height and 100 mm of diameter, with a nozzle placed at the bottom, as shown in Fig. 1. Two conditions at the tube wall were investigated. Firstly, an average convective coefficient of $h = 25\ W\ m^{-2}\ K^{-1}$ is proposed to simulate the heat transfer between the reactor and the outside environment, and secondly, the wall is considered adiabatic, to study the influence of thermal insulation on the reactor temperature and carbon black formation. Furthermore, additional simulations were performed including the air surrounding the reactor, to verify the adequacy of the proposed convective coefficient. In that sense, an extended domain was considered (mesh with ~250.000 cells), which increased the total domain by 100 mm around the whole reactor and included the 3 mm thick glass wall.

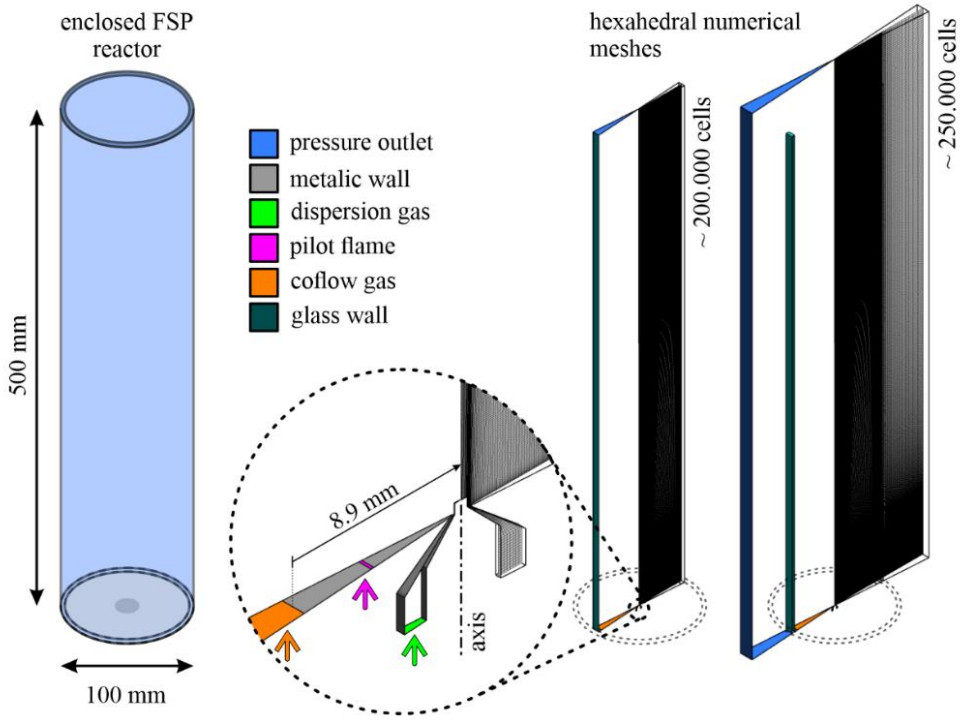

Fig. 1: Enclosed FSP reactor geometry and numerical meshes.

The present simulations consider an injection of 5 mL/min of fuel that is dispersed by 5 L/min of pure nitrogen (N_2). The initial size distribution of the droplets in the spray is represented by a Rosin-Rammler-Sperling-Bennet (RRSB) distribution. The pilot flame is composed of a mixture of methane (19% mass) and oxygen (81% mass).

The fuel is composed of pure p-xylene (C_8H_{10}) and its liquid and gaseous properties are taken from the works of Yaws [27], [28]. Two chemical reactions are present, the direct combustion of p-xylene and of methane which generates water (H_2O) and carbon dioxide (CO_2). The mathematical modeling and CFD approach used in this work are based on the works of Noriler et. al [29], [30], and Bianchi Neto et. al [26], [31], with one-step reaction mechanisms for combustion. The carbon black formation kinetics is explained in detail in the next section.

2.1. Carbon black kinetics

Here we adapt the mathematical modeling approach proposed by Boulanger et. al [5], in which a three-equation model is solved to determine the mass fraction and size profiles of particles along the reactor. The model is based on the two-equation model developed by Tesner et. al [6], where the authors' main contribution is to include a term for superficial growth of the soot particles, connecting fuel concentration and soot mass growth. The equations for Boulanger's model are presented below:

$$\frac{d(\rho y_s)}{dt} = K_{G,incep} N_F + C_a an - N A_s S_{ox} \tag{1}$$

$$\rho \frac{dn}{dt} = a_0 N_F \exp\left(\frac{-T_{a_{n_o}}}{T}\right) + Fn - g_0 Nn - S'_{ox} \tag{2}$$

$$\rho \frac{dN}{dt} = an - bNn - K_c \sqrt{T} \left(\frac{\rho y_s}{\rho_s}\right)^{\frac{1}{6}} N^{\frac{11}{6}} \tag{3}$$

Where $K_{G,incep}$ is the nucleation constant, N_F is the numeric concentration of fuel, C_a is the initial soot particle mass, like the superficial particle area, S_{ox} and S'_{ox} are oxidation rates of particles and nuclei, which are described in detail by Boulanger et. al [5]. The constant a_0 is given as the vibration frequency of the bond to be broken, K_C is the coagulation coefficient, ρ_s is soot's density, and a, g_0, F, and b are mathematical constants from the model.

Eq. (1) refers to soot mass fraction y_s and its first term on the right-hand side refers to the superficial growth of particles. The second term on the right-hand side refers to the formation that arises from radical nuclei, and the last one is related to particle oxidation. Eq. (2) refers to the formation rate of radical nuclei, where the first term on the right-hand side represents the nuclei formation by fuel pyrolysis, and the second and third ones refer to the radical nuclei number growth through chain branching and destruction when landing on soot particles, respectively. Eq. (3) refers to the number density of soot particles, where the first and the second terms on the right-hand side are related to the numeric formation and termination of particles, respectively, and the last one refers to the coalescence process (as proposed by Fusco et. al [4]). The model has been implemented in ANSYS Fluent 19.2 through the use of user-defined functions (UDFs) as an adaptation of the already available two-step model (based on the work of Tesner et. al [6], [32]).

The influence of particle's radiation in the process is taken into account by the model proposed by Sazhin [33], the gas absorption coefficient is calculated by Eq. (4),

$$a_s = b_1 \rho y_s [1 + b_T (T - 2000)] \tag{4}$$

whereas is the soot absorption coefficient, b_1 and b_T are model constants (b_1 = 1232.4 $m^2 kg^{-1}$ and b_T = 4.8e^{-4} K^{-1}). ρ, y_s and T are local gas densities, carbon black mass fraction, and gas temperature, respectively. Results, where particle's radiation is neglected, are shown in the next section.

3. Results and Discussion

3.1 Temperature

The results for temperature obtained in the simulations are presented in Fig. 2. In the contour presented on the left-hand side of the figure, a significant temperature difference is observed between the adiabatic and non-adiabatic cases, as expected. On the right-hand side, at the plot of temperature over the rector centerline, it is noticeable that the reactor, for the adiabatic case, is kept at high temperatures (higher than 1200 K) at the entire domain. The temperature peak for both cases is, however, very similar, at ~2500 K, which is because this region in the center is where most of the combustion occurs. The comparison between the results for the regular and extended meshes is also shown in the plot. As it is observed, the lines almost overlap showing that very similar results are obtained. These results show that the proposed value for the convective coefficient provides a satisfactory approximation, which is interesting given that the smaller mesh requires a lower computational cost for the solution.

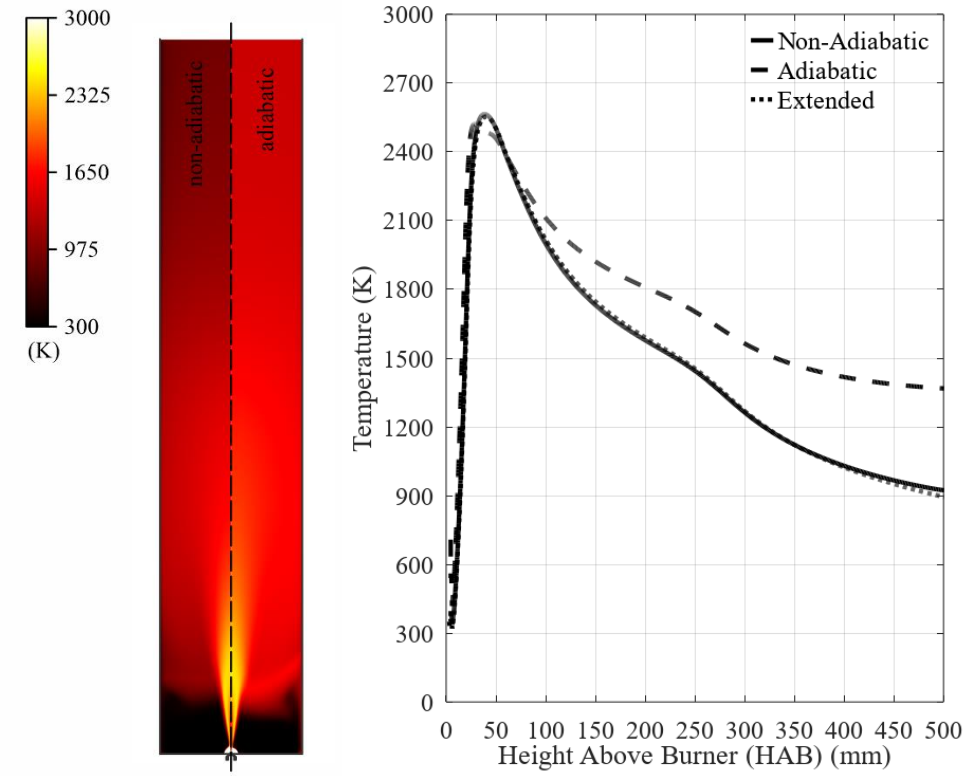

Fig. 2: Temperature contour (left) and profiles along the centerline for considered cases (right): non-adiabatic with regular (solid line) and extended meshes (dotted line) and adiabatic (dashed line).

3.2 Carbon Black

In Figs. 3 and 4, the results concerning carbon black formation and evolution inside the reactor are presented for the adiabatic and non-adiabatic cases. The presented profiles are values radially averaged along with the reactor height. The model proposed for the nanoparticles showed to be highly sensitive to temperature and composition profiles. The normalized concentration of radical nuclei, shown in Fig. 3, is mostly affected by the oxidation rates, which are the greatest in the lower regions of the reactor where the combustion takes place. The number concentration of nanoparticles, also shown in Fig. 3, presents a significant divergence between the studied cases.

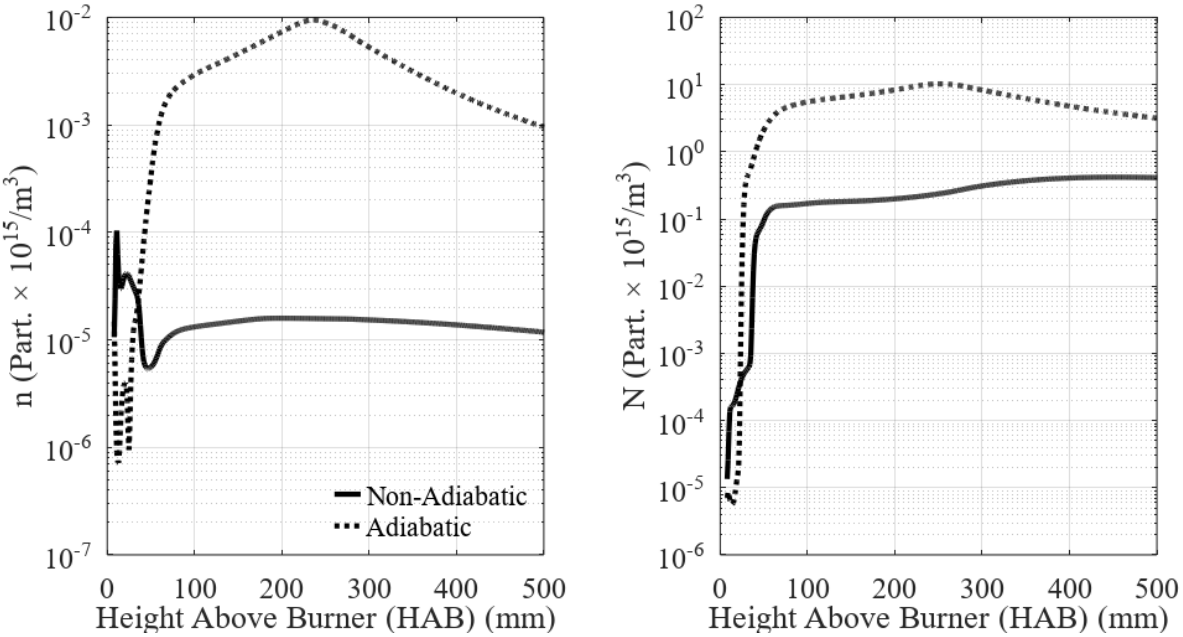

Fig. 3 – Profiles of normalized nuclei concentration (left) and normalized particle number concentration (right): non-adiabatic (solid line) and adiabatic (dotted line).

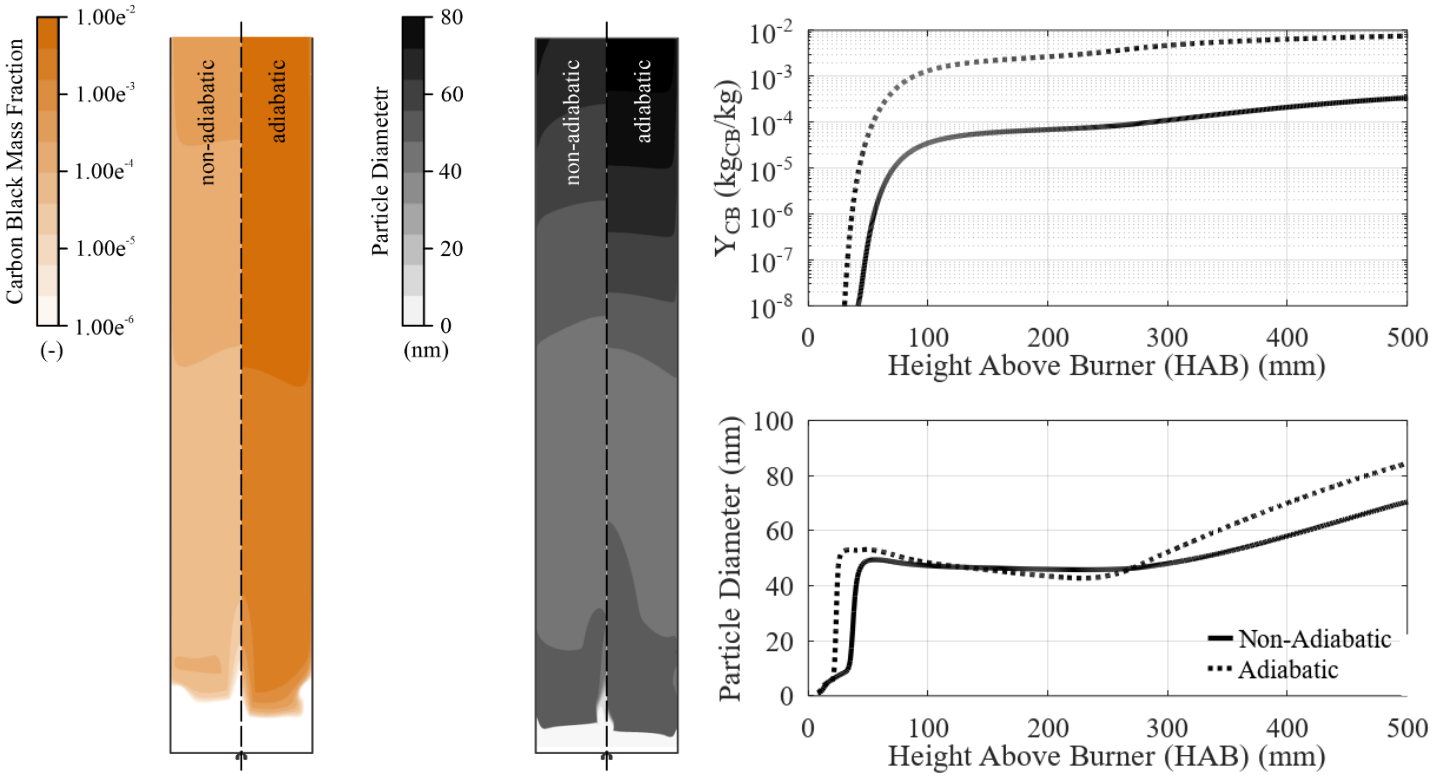

Fig. 4 – Contours of carbon black mass fraction and particle diameter (left) and profiles along with reactor height (right): non-adiabatic (solid line) and adiabatic (dotted line).

The higher temperatures observed in the adiabatic case increase the nucleation rates inside the domain, causing the concentration of nuclei to increase in the lower region of the reactor. The higher concentration of nuclei, in turn, increases the number concentration of carbon black.

Contours of particle diameter and carbon black mass fraction are presented in Fig. 4, accompanied by the profiles throughout the reactor. The mass fraction of carbon black follows the previous trend observed for the particle number concentration. The higher concentration of carbon black in the adiabatic case, as mentioned, is due to the increased nucleation and chain branching rates due to the higher temperature. The results for particle diameter show agreement with what is described in the literature [22]. In the hotter regions, the mean particle size tends to decrease due to the high number of newly generated particles (peak of nuclei concentration). At 250 mm HAB, nuclei concentration and inception of new particles decrease quickly, and the particle's diameter returns to grow according to the superficial growth term of the model.

3.3 Influence of Particle Radiation

When studying the formation of soot and carbon black, the modeling of particle-radiation interaction, as described in Eq. (4), is important to avoid overestimations of flame temperature, which could affect the nanoparticle formation kinetics. In Fig. 5, results comparing cases with and without this phenomenon are presented. For the adiabatic case, particle radiation has a very significant effect on the carbon black mass fraction produced inside the reactor. This is caused by an increase in the nucleation rate, generating more nuclei, which increases its chain branching process. The non-adiabatic case, on other hand, presents very low variation between the profiles, due to the relatively small carbon black production in this case. A significant temperature profile is observed only for the adiabatic case, due to high quantities of carbon black mass fraction, which affects the radiation model employed (Eq. (4)).

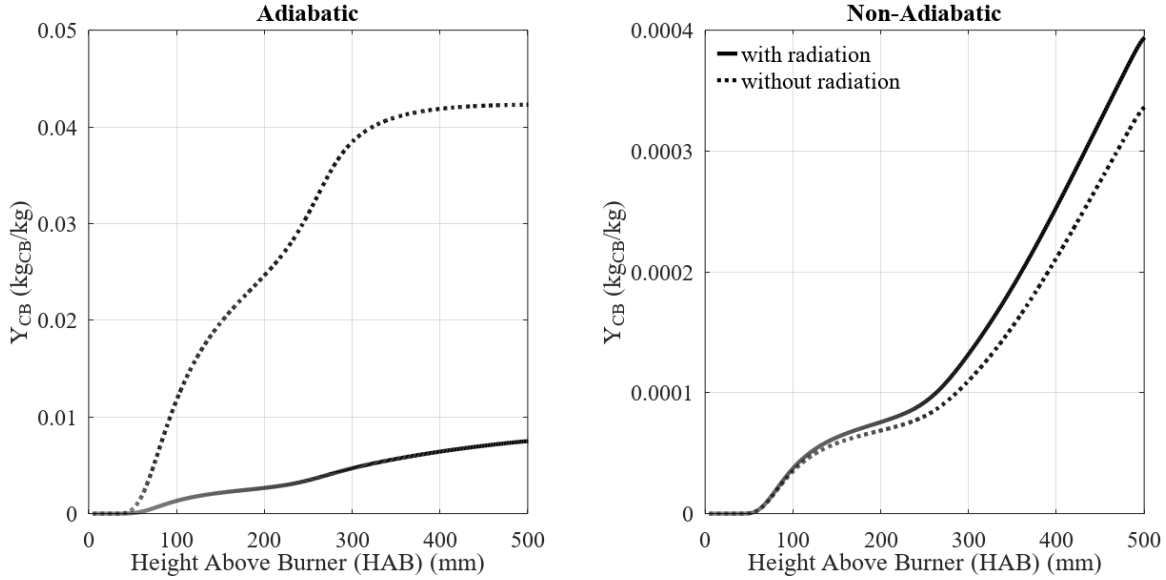

Fig. 5 – Profiles of carbon black mass fraction for the non-adiabatic (left) and the adiabatic (right) cases: with particle radiation (solid line) and without particle radiation (dashed line).

4. Conclusion

In this work, CFD simulations of the production of carbon black via the FSP process were carried out, coupled with a monodisperse PBM. Initial results showed that the use of an average value for the convective coefficient at the reactor walls is appropriate, avoiding the need for the discretization of the air surrounding the reactor. This simplification reduces the final size of the numerical mesh, cheapening the necessary computational cost.

Additional results indicated that with the use of thermal insulation in the reactor walls, a much higher temperature profile is observed. The effects of this hotter domain on the final particle diameter are not very significant, the final quantity of the

material, however, is greater, given that the temperature directly influences the nucleation and oxidation rates of the carbon black. In that sense, the practice of insulating the reactor has the potential for process design allowing for a more controlled quenching of the system.

Finally, the influence of particle radiation on the final product was meant only for the adiabatic case, given the high concentrations of the nanomaterial in the reactor. This phenomenon, however, should be further investigated and experimental data should be used for model validation.

Acknowledgments

This study received funding from the São Paulo Research Foundation – FAPESP (Project ID: 2020/08502-9 and 2021/01067-8), in Brazil. Additional acknowledgment is also directed to the Coordination of Higher Educational Personnel – CAPES (Process ID: BEX 12369/12-8).

References

[1] I. . Khan, G. Greeves, and D. . Probert, *Air Pollution Control in Transport Engines*. London: The Institution of Mechanical Engineers, 1971.

[2] H. Hiroyasu, T. Kadota, and M. Arai, "Development and Use of a Spray Combustion Modeling to Predict Diesel Engine Efficiency and Pollutant Emissions : Part 1 Combustion Modeling," *Bull. JSME*, vol. 26, no. 214, pp. 569–575, 1983, doi: 10.1299/jsme1958.26.569.

[3] P. S. Mehta and S. Das, "A correlation for soot concentration in diesel exhaust based on fuel-air mixing parameters," *Fuel*, vol. 71, no. 6, pp. 689–692, Jun. 1992, doi: 10.1016/0016-2361(92)90173-L.

[4] A. Fusco, A. L. Knox-Kelecy, and D. E. Foster, "Application of a phenomenological soot model for diesel engine combustion," in *The 3rd International Symposium on Diagnostics and Modeling of Combustion in Internal Combustion Engines*, 1994, pp. 571–576.

[5] J. Boulanger, F. Liu, W. S. Neill, and G. J. Smallwood, "An improved soot formation model for 3D diesel engine simulations," *J. Eng. Gas Turbines Power*, vol. 129, no. 3, pp. 877–894, Jul. 2007, doi: 10.1115/1.2718234.

[6] P. A. Tesner, T. D. Smegiriova, and V. G. Knorre, "Kinetics of dispersed carbon formation," *Combust. Flame*, vol. 17, no. 2, pp. 253–260, Oct. 1971, doi: 10.1016/S0010-2180(71)80168-2.

[7] I. M. Kennedy, W. Kollmann, and J. Y. Chen, "A model for soot formation in a laminar diffusion flame," *Combust. Flame*, vol. 81, no. 1, pp. 73–85, Jul. 1990, doi: 10.1016/0010-2180(90)90071-X.

[8] M. Frenklach and H. Wang, "Detailed modeling of soot particle nucleation and growth," *Symp. Combust.*, vol. 23, no. 1, pp. 1559–1566, 1991, doi: 10.1016/S0082-0784(06)80426-1.

[9] S. J. Brookes and J. B. Moss, "Predictions of soot and thermal radiation properties in confined turbulent jet diffusion flames," *Combust. Flame*, vol. 116, no. 4, pp. 486–503, 1999, doi: 10.1016/S0010-2180(98)00056-X.

[10] Z. Wen, S. Yun, M. J. Thomson, and M. F. Lightstone, "Modeling soot formation in turbulent kerosene/air jet diffusion flames," *Combust. Flame*, vol. 135, no. 3, pp. 323–340, Nov. 2003, doi: 10.1016/S0010-2180(03)00179-2.

[11] M. Frenklach and H. Wang, "Detailed mechanism and modeling of soot particle formation," in *Soot Formation in Combustion*, B. H., Ed. Springer Berlin Heidelberg, 1994.

[12] M. Frenklach, "A Unifying Picture of Gas-Phase Formation and Growth of PAH, Soot, Diamond, and Graphite," in *Carbon in the Galaxy: Studies from Earth and Space*, Aug. 1990, no. 3061, p. 259, DOI: 10.1002/chin.199145318.

[13] D. R. Tree and K. I. Svensson, "Soot processes in compression ignition engines," *Prog. Energy Combust. Sci.*, vol. 33, no. 3, pp. 272–309, Jun. 2007, doi: 10.1016/j.pecs.2006.03.002.

[14] H. Omidvarborna, A. Kumar, and D. S. Kim, "Recent studies on soot modeling for diesel combustion," *Renew. Sustain. Energy Rev.*, vol. 48, pp. 635–647, 2015, doi: 10.1016/j.rser.2015.04.019.

[15] H. Yuan, W. Kong, F. Liu, and D. Chen, "Study on soot nucleation and growth from PAHs and some reactive species at flame temperatures by ReaxFF molecular dynamics," *Chem. Eng. Sci.*, vol. 195, pp. 748–757, Feb. 2019, doi: 10.1016/j.ces.2018.10.020.

[16] A. Y. Watson and P. A. Valberg, "Carbon black and soot: Two different substances," *Am. Ind. Hyg. Assoc. J.*, vol. 62,

no. 2, pp. 218–228, 2001, DOI: 10.1080/15298660108984625.
[17] G. Xia, J. Ye, Z. Zheng, X. Li, C. Chen, and C. Hu, "Catalytic FeP decorated carbon black as a multifunctional conducting additive for high-performance lithium-sulfur batteries," *Carbon N. Y.*, vol. 172, pp. 96–105, Feb. 2021, doi: 10.1016/j.carbon.2020.09.094.
[18] X. Yi, X. He, F. Yin, B. Chen, G. Li, and H. Yin, "Co-CoO-Co3O4/N-doped carbon derived from metal-organic framework: The addition of carbon black for boosting oxygen electrocatalysis and Zn-Air battery," *Electrochim. Acta*, vol. 295, pp. 966–977, Feb. 2019, doi: 10.1016/j.electacta.2018.11.142.
[19] X. Wu, M. Liu, S. Yao, S. Li, S. Pang, X. Shen, T. Li and S. Qin, "Boosting the electrochemical performance of lithium-sulfur batteries by using a carbon black/LiMn2O4-modified separator," *J. Alloys Compd.*, vol. 835, p. 155251, Sep. 2020, doi: 10.1016/j.jallcom.2020.155251.
[20] J.-B. Donnet, R. C. Bansal, and M.-J. Wang, *Carbon Black: Science and Technology*, 2nd ed. Taylor & Francis, 1993.
[21] W. Y. Teoh, R. Amal, and L. Mädler, "Flame spray pyrolysis: An enabling technology for nanoparticles design and fabrication.," *Nanoscale*, vol. 2, no. 8, pp. 1324–47, Aug. 2010, doi: 10.1039/c0nr00017e.
[22] C. O. Okoye, I. Jones, M. Zhu, Z. Zhang, and D. Zhang, "Manufacturing of carbon black from spent tyre pyrolysis oil – A literature review," *J. Clean. Prod.*, vol. 279, p. 123336, 2021, doi: 10.1016/j.jclepro.2020.123336.
[23] M. Ciobanu, A.-M. Lepadatu, and S. Asaftei, "Chemical and Electrochemical Studies of Carbon Black Surface by Treatment with Ozone and Nitrogen Oxide," *Mater. Today Proc.*, vol. 3, pp. S252–S257, Jan. 2016, doi: 10.1016/j.matpr.2016.02.042.
[24] E. B. Sebok and R. L. Taylor, "Carbon Blacks," in *Encyclopedia of Materials: Science and Technology*, vol. 24, no. 6, Elsevier, 2001, pp. 902–906.
[25] F. Meierhofer, L. Mädler, and U. Fritsching, "Nanoparticle evolution in flame spray pyrolysis—Process design via experimental and computational analysis," *AIChE J.*, vol. 66, no. 2, pp. 1–14, Feb. 2020, doi: 10.1002/aic.16885.
[26] P. Bianchi Neto, L. Buss, F. Meierhofer, H. F. Meier, U. Fritsching, and D. Noriler, "Combustion kinetic analysis of flame spray pyrolysis process," *Chem. Eng. Process. - Process Intensif.*, vol. 129, no. April, pp. 17–27, 2018, doi: 10.1016/j.cep.2018.04.032.
[27] C. L. Yaws, *Thermophysical Properties of Chemicals and Hydrocarbons*, 2nd ed. Oxford, UK: Elsevier, 2014.
[28] C. L. Yaws, *The Yaws Handbook of Physical Properties for Hydrocarbons and Chemicals*, 2nd ed. Oxford, UK: Elsevier, 2015.
[29] D. Noriler, C. D. Rosebrock, L. Mädler, H. F. Meier, and U. Fritsching, "Influence of atomization and spray parameters on the flame spray process for nanoparticle production," *At. Sprays*, vol. 24, no. 6, pp. 495–524, 2014, doi: 10.1615/AtomizSpr.2014008559.
[30] D. Noriler, M. J. Hodapp, R. K. Decker, H. F. Meier, F. Meierhofer, and U. Fritsching, "Numerical Simulation of Flame Spray Pyrolysis Process for Nanoparticle productions: effects of 2d and 3d approaches," *ASME*, pp. 1–9, 2014.
[31] P. Bianchi Neto, F. Meierhofer, H. F. Meier, U. Fritsching, and D. Noriler, "Modelling polydisperse nanoparticle size distributions as produced via flame spray pyrolysis," *Powder Technol.*, vol. 370, pp. 116–128, Jun. 2020, doi: 10.1016/j.powtec.2020.05.019.
[32] ANSYS, *ANSYS Fluent Theory Guide*, Release 15. Canonsburg: ANSYS Inc., USA, 2013.
[33] S. S. Sazhin, "An approximation for the absorption coefficient of soot in a radiating gas," *Fluent Eur.*, 1994.